Interplay between Molecular Diffusion and Advection during Solute Transport in Macroporous Media

Stéphane Batany, Pierre-Emmanuel Peyneau, Laurent Lassabatère, Beatrice Bechet, Pamela Françoise Faure, Patrick Dangla

Published May 31, 2019

Special Section: Nonuniform Flow across Vadose Zone Scales

Core Ideas

- BTCs in a macroporous medium cannot always be fitted by classical transport models.
- Classical transport models can be faulted in a simple heterogeneous porous medium.
- Molecular diffusion affects solute transport for sufficient mean residence time.
- The shape of the BTCs depends on the mean residence time of the solute.

Interplay between Molecular Diffusion and Advection during Solute Transport in Macroporous Media

Stéphane Batany, Pierre-Emmanuel Peyneau,* Laurent Lassabatère, Béatrice Béchet, Paméla Faure, and Patrick Dangla

Solute transport in soils is known to differ from solute transport in homogeneous porous media. Nonequilibrium processes, like those induced by the presence of macropores, can strongly influence the breakthrough of solute in soils. Breakthrough experiments and effective models are often combined to study the physicochemical processes involved in solute transport. However, the complexity of flow pathways and the diversity of possible processes is challenging. In this work, the influence of flow rate and viscosity of the carrying liquid on nonreactive solute transport is investigated under saturated conditions in a macroporous synthetic medium. As expected, solute transport is strongly affected by physical nonequilibrium induced by the preferential flow within the macropore. Breakthrough occurs early, and the shape of the breakthrough curve is influenced both by the flow rate and the coefficient of molecular diffusion of the solute. We show that when the mean residence time of the solute in the macropore is small enough, solute transport in a macroporous column can be considered as isolated within the macropore. The increase of the residence time strongly affects the shape of the breakthrough, and, eventually, a plateau appears during the ascent of the breakthrough curve. We demonstrate experimentally that the existence of this plateau, which is not predicted by classical effective models, is related to the relative importance of molecular diffusion versus advection. Indeed, this plateau can become unobservable if the coefficient of molecular diffusion is reduced through the use of a sufficiently viscous carrying liquid.

Abbreviations: BTC, breakthrough curve; CDE, convection–dispersion equation; DPM, dual-permeability model; MIM, mobile–immobile model.

S. Batany, P.-E. Peyneau, and B. Béchet, IFSTTAR, GERS, EE, F-44340 Bouguenais, France; L. Lassabatère, Univ. de Lyon, UMR 5023 LEHNA, Université Lyon 1, École Nationale des Travaux Publics de l'État, Centre National de la Recherche Scientifique, 3 rue Maurice Audin, 69518 Vaulx-en-Velin, France; P. Faure and P. Dangla, Univ. Paris-Est, Lab. Navier, F-77455 Marne-la-Vallée, France. *Corresponding author (pierre-emmanuel.peyneau@ifsttar.fr).

Received 28 July 2018.
Accepted 27 Jan. 2019.

Citation: Batany, S., P.-E. Peyneau, L. Lassabatère, B. Béchet, P. Faure, and P. Dangla. 2019. Interplay between molecular diffusion and advection during solute transport in macroporous media. Vadose Zone J. 18:180140. doi:10.2136/vzj2018.07.0140

Macropores enhance water flow and contaminant transport in soils. They may result from biological activity (e.g., earthworm holes, degradation of roots) or from physical processes (e.g., cracks, fissures) (Beven and Germann, 1982, 2013). Numerous field studies have shown that some preferential flow occurs through earthworm holes or root channels present in soils (Larsson et al., 1999). Macropores thus form preferential pathways for water, as well as solutes and particles within water, from the vadose zone and down to groundwater (Beven and Germann, 1982, 2013; Zehe and Flühler, 2001). These bypasses shorten the contact time between contaminants and the soil matrix and may harm the filtering function of the soil (Lamy et al., 2013; Lassabatere et al., 2004).

However, soils have different types of macropores, and their macroporosity is not necessarily entirely activated, even after an intense rainfall. Preferential flow observed on the field or even with undisturbed soil columns (Seyfried and Rao, 1987; Vanderborght et al., 2000) results from a combination of different but hardly distinguishable heterogeneities. To better understand the role played by an individual macropore, various approaches have been undertaken (Allaire et al., 2009; Rosenbom et al., 2009; Vanderborght et al., 2002; Vogel et al., 2006). Different artificial systems have provided several insights into the mechanisms involved in macropore flow, such as uniformly packed soils containing constructed macropores (Czapar et al., 1992; Ghodrati et al., 1999; Lamy et al., 2009; Li and Ghodrati, 1997), or macroporous glass micromodels (Phillips et al., 1989; Wan et al.,

1996). Modeling and numerical simulations have also been used to clarify the complex interplay existing between water flux, the fraction of the pore space filled by mobile water, and contaminant transport within the macropore and the surrounding matrix (Allaire et al., 2002; Gerke and Köhne, 2004; Saravanathiiban et al., 2014; Weiler, 2005).

Breakthrough experiments performed in experimental columns have provided valuable information on contaminant transport in macroporous soils (Griffioen et al., 1998). Early breakthrough is routinely spotted on these systems and reflects the existence of a preferential water flow. However, many processes can affect the transport of contaminants, and their fate cannot be easily determined at the pore scale because of the geometrical complexity of any soil sample.

To handle this complexity issue, several types of effective (upscaled) mathematical models have been developed to simulate solute transport in soils at a scale greater than the pore scale (Gerke, 2006; Köhne et al., 2009). Frequently used models in soil physics include the classical convection–dispersion equation (CDE) and various non-equilibrium models, such as the mobile–immobile model (MIM)—sometimes called two-region model or dual-porosity model—and the dual-permeability model (DPM). More sophisticated stochastic models based on a continuous-time random walk can also be used, especially in a hydrogeological context (Berkowitz and Scher, 2009; Berkowitz et al., 2006, 2008; Bijeljic and Blunt, 2006). The validity of these models is generally assessed on the agreement between measured and simulated breakthrough curves (BTCs), and fitted parameters are assumed to reflect soil properties, such as the dispersivity, the transfer rate coefficient, or the extent of the mobile region (Lafolie et al., 1997). Despite their rich phenomenology, BTCs contain a limited amount of information and cannot provide a clear-cut answer concerning the whole set of transport processes involved in a given soil column (Brusseau and Rao, 1990; van Genuchten and Wierenga, 1976). Furthermore, various studies have stressed that effective parameters may vary with flow rate or the size of the system (Griffioen et al., 1998; Khan and Jury, 1990; Lafolie et al., 1997). These variations may be due to the parameter non-uniqueness issue plaguing non-equilibrium effective models, but they can also reflect the lack of physical soundness of the chosen model itself.

We thus believe that there is room for improvement in the understanding of flow and contaminant transport in macroporous soils, even for nonreactive solutes flowing along water streamlines, which are the simplest contaminants to deal with. At the smallest scale where continuum mechanics still holds, the transport of these solutes is driven by only two physical processes: advection induced by the water velocity field and molecular diffusion of the solute. A few attempts have been made to go beyond effective models for the simulation of nonreactive solute transport and to describe on a physically sound basis either the velocity field within a macropore (Di Pietro et al., 2003; Perret et al., 2000) or solute transport with the diffusion equation. Rao et al. (1980a, 1980b, 1982) considered for instance diffusive transport in a porous medium made of spherical aggregates, whereas van Genuchten et al. (1984) and Cihan and Tyner (2011) studied diffusive transport within a homogeneous porous media containing a cylindrical hollow along its axis. Previous studies have examined the simultaneous effect of advection and molecular diffusion for stratified or fractured porous media (Neretnieks, 1980; Sudicky et al., 1985; Tang et al., 1981); however, in soil physics, with a few exceptions (Brusseau, 1993; Hu and Brusseau, 1995), the velocity field and molecular diffusion are generally overlooked, and the effect of small-scale variability on macroscopic solute transport is described statistically through the use of the coefficient of longitudinal dispersion or the dispersion tensor. In this paper, we show that the molecular diffusion coefficient of the solute can influence nonreactive solute transport in macroporous media at a very early stage. To highlight the role played by molecular diffusion on solute transport, we worked under saturated conditions. Indeed, when a soil sample containing a single macropore undergoes a leaching experiment under steady unsaturated conditions, the region of the pore space filled by water can display a complex shape. For instance, a film flow along the boundary of the macropore is sometimes observed even when water is under tension within the system (Wan et al., 1996). Other factors that are not easily quantifiable, such as air bubbles entrapped near the matrix–macropore interface, variations in water matrix potential, or surface roughness, may also affect water flow and solute transport (Phillips et al., 1989). Working under saturated conditions allows a better understanding of the liquid velocity field. This detailed knowledge is important to disentangle advective and diffusive contributions to nonreactive solute transport.

In this study, we determined the breakthrough of KBr in two saturated columns (one with a macropore, one homogeneous) filled with a synthetic material made of glass beads. Our goal was to study nonreactive solute transport in these columns and to get a better grasp of the role played by solute exchange between the macropore and the neighboring porous matrix under saturated conditions for different flow rates and with two distinct saturating liquids (pure water and a much more viscous glycerol–water mixture). We can independently adjust these two factors to weigh the relative importance of advective and diffusive transport processes. For instance, the relative importance of transport by advection can be boosted in two different and independent ways: (i) by increasing the flow rate or (ii) by increasing the viscosity of the carrying liquid, thus reducing the coefficient of molecular diffusion of the solute.

Here we start by describing some theoretical considerations on water flow and solute transport in macroporous columns. The experimental columns made of glass beads (one with a macropore, one homogeneous) are presented, along with the Br^- breakthrough experiments performed for steady flow rates varying over two orders of magnitude. The analysis of the BTCs is described, and the BTCs measured on the macroporous column, first with aqueous solutions and then with glycerol–water solutions, are presented. The purpose of the glycerol–water solutions is to decrease the coefficient of molecular diffusion of the Br^- ion and, consequently,

to reduce the mass exchange between the macropore and the surrounding porous matrix. The BTCs of the macroporous column are compared with those measured at the outlet of a nonporous straight pipe of circular cross-section having the same diameter and length than the macropore. The wall of the pipe ensures that no solute can exit the macropore (except at the outlet) and simulates the limiting case where any mass exchange between the macropore and its surroundings is prohibited. The paper ends with a discussion of the respective contributions of advection and molecular diffusion to nonreactive solute transport in macroporous media and some thoughts on potential research directions.

Theoretical Considerations and Implications for Transport Modeling

We consider a macroporous column of diameter d_{col}, filled with a homogeneous porous medium made of nonporous round shaped grains of mean diameter d_g, except along the axis of the column where there is a cylindrical macropore of diameter d_{macro} (Fig. 1a). The diameter of the macropore is assumed to be at least equal to a few grain sizes ($d_{macro} \geq 5d_g$) and much less than the diameter of the column ($d_{macro} << d_{col}$). Under these assumptions, when the system is saturated by a Newtonian liquid like water and submitted to a moderate steady flow rate, the velocity profile within the macropore, in a plane perpendicular to its axis, is expected to be approximately parabolic. Indeed, if the macropore were bounded by a cylindrical wall, and with a steady flow rate sufficiently gentle for the flow to stay laminar, the liquid velocity field would obey Poiseuille's law, and the velocity profile would be perfectly parabolic. However, in our case, the macropore is bounded by some grains that are part of the surrounding homogeneous porous medium, and Poiseuille's law is not strictly verified.

Water flow at the interface between a zone without any particle (free flow channel) and a porous material has received a great deal of attention, especially in the context of fractured porous media (Berkowitz, 1989). It has been shown experimentally that a Newtonian liquid flowing in a channel parallel to a porous

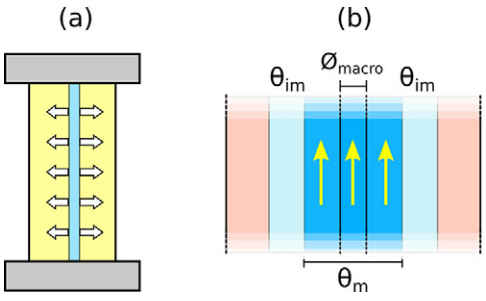

Fig. 1. (a) Mass exchange at the interface between the macropore (diameter d_{macro}, in blue) and the surrounding porous matrix (in yellow) in a macroporous column; (b) expected mobile–immobile modeling for a macroporous column: the mobile region encompasses the macropore and its surroundings, and the immobile region is a fraction of the pore space within the bulk of the porous matrix. θ_{im}, water content of the immobile phase; θ_m, water content of the mobile phase.

medium can affect the flow in the porous medium close to the interface because of the viscous shear exerted by the liquid moving in the channel on the liquid located between the grains lining the channel. Beavers and Joseph (1967) proposed a mathematical model to account for this phenomenon, in which a slip boundary condition is assumed to hold at the interface. The extension of the transition region of disturbed flow in the porous media has been studied theoretically (Berkowitz, 1989) and experimentally (Arthur et al., 2009; Wan et al., 1996). It appears that for a model porous media mimicking a soil, the thickness of the transition region is very small (at most a few d_g). Darcy's law is not applicable in this small transition region but can be assumed to hold for the flow in the remainder of the porous medium. Furthermore, the experiments of Arthur et al. (2009) and Wan et al. (1996) show that the velocity profile in the channel retains a classical parabolic shape reminiscent of the profile obtained for laminar flow in a straight channel.

If the transition region is neglected, one can assume that the flow within the macroporous column is the superposition of a quasi-Poiseuille flow in the macropore and a Darcian flow in the porous matrix of porosity φ (pore volume of the matrix divided by its total volume and permeability k_{mat}). It is well known that the flow rate of a Poiseuille flow can be represented by Darcy's law: a permeability k_{macro} can thus be assigned to the liquid saturated macropore. Under these approximations, the flow in the column is the juxtaposition of two Darcian flows in parallel and the ratio of pore velocities between the matrix and the macropore, which is independent of the value of the flow rate, is

$$\frac{v_{mat}}{v_{macro}} = \frac{1}{\phi}\frac{k_{mat}}{k_{macro}} \quad [1]$$

The application of Poiseuille's law in the cylindrical macropore gives $k_{macro} = d^2_{macro}/32$ (Bear, 1972). Moreover, according to the Kozeny–Carman relation, the permeability of the matrix can be considered to be close to $k_{mat} = d_g{}^2\varphi^3/[180(1-\varphi)^2]$ (Bear, 1972). Consequently,

$$\frac{v_{mat}}{v_{macro}}; \quad \frac{\phi^2}{6(1-\phi)^2}\frac{d_g^2}{d_{macro}^2} \quad [2]$$

The porosity of a random packing of polydisperse spheres with a polydispersity index

$$\sqrt{\left\langle (r-\langle r\rangle)^2 \right\rangle}\Big/\langle r\rangle \leq 0.40$$

ranges between 0.32 and 0.36 (Desmond and Weeks, 2014; Farr and Groot, 2009), so, according to Eq. [2], v_{mat}/v_{macro} essentially scales as $(d_g/d_{macro})^2$. Because $d_{macro} \geq 5d_g$, the order of magnitude of this ratio is $O(10^{-3})$.

The order of magnitude of v_{mat}/v_{macro} is of paramount importance if one wants to select an effective model for solute transport on physical grounds. The column being obviously heterogeneous, in addition to CDE, at least two possible effective models come to mind: the MIM and the DPM. The MIM should not be discarded

in favor of DPM because of the existence of a nonzero mean velocity, either in the macropore or within the porous matrix (Eq. [2]). Indeed, the immobile region may contain water that is stagnant, as assumed in the seminal work of Coats and Smith (1964), or it may contain water that is flowing much slower than that in the mobile region, rendering the immobile water effectively stagnant.

Experiments with porous micromodels designed to simulate solute transport in an aggregated soil rather suggest that the MIM is able to accurately reproduce the effluent curves provided that the velocity ratio between the "slow" region and the "fast" region (v_{mat}/v_{macro} in our case) is small enough ($\leq 10^{-3}$) (Zinn et al., 2004). On the other hand, effluent curves can be well fitted with a CDE when the velocity ratio is high enough (velocity ratio ≥ 0.2) or when the residence time is sufficiently long for the concentrations in both domains to equilibrate. The situation is more involved for an intermediate velocity ratio: Zinn et al. (2004) had to resort to a dedicated upscaled transport model to properly fit the effluent curves obtained in this case.

Given that $v_{mat}/v_{macro} = O(10^{-3})$ for the kind of macroporous column herein considered, the MIM is presumptively more suited than DPM or CDE to reproduce experimental BTCs. Consequently, BTCs will be systematically fitted with the MIM, and a CDE fit will be displayed for the sake of comparison. The order of magnitude of v_{mat}/v_{macro} also enables making a reasonable prediction for the fraction of mobile water: the mobile region should likely encompass the macropore and possibly its immediate surroundings, whereas the immobile region should be a fraction of the pore space belonging to the porous matrix (Fig. 1 depicts the conceptual model considered in this study). Therefore, if the MIM is physically relevant to simulate solute transport in the macroporous column, we expect to find that the fraction of mobile water is roughly equal to the fraction of the pore space occupied by the macropore.

The diffusive component of solute transport, which is expected to affect mass transfer between mobile and immobile regions, can be altered by modifying the viscosity of the saturating liquid. According to Stokes–Einstein law, the molecular diffusion coefficient D_0 of a solute is inversely proportional to the viscosity of the liquid, $D_0 = k_B T/(6\pi\mu r)$, where k_B is the Boltzmann constant, T is the thermodynamic temperature, μ is the dynamic viscosity of the fluid, and r is the hydrodynamic radius of the diffusive solute (Li and Chang, 1955). Thus, at a given flow rate, the mass transfer coefficient is expected to decrease when increasing the viscosity of the saturating liquid.

Materials and Methods

Porous Media

We constructed two experimental acrylic glass columns (one with a macropore and the other one homogeneous) filled with a synthetic consolidated porous medium made of spherical glass beads with a diameter uniformly distributed between 0.4 and 0.8 mm ($d_g = 0.6$ mm, polydispersity index of 0.18). Consolidation has been achieved with an epoxy resin (Araldite) during the fabrication of the porous medium, ensuring that its structure remains unchanged even if the system undergoes a succession of breakthrough experiments. The diameter of each column is 5.0 cm ($d_{col} \cong 84\, d_g$), and the height of each column is $L_{col} = 14.5$ cm.

A macroporous column (Column M) was constructed by inserting a 3-mm-diameter Teflon cylindrical rod along the axis of the column before the insertion of the mixture of beads and glue. The rod was removed as soon as the medium was sufficiently consolidated (Column M is shown schematically in Fig. 2b). The presence of the glue prevents the collapse of the macropore during the breakthrough experiments (macropore collapse often represents a major impediment for breakthrough experiments performed in engineered columns [Li and Ghodrati, 1997]). The constructed macropore has a volume of 1.5 mL because its effective diameter d_{macro} is equal to the rod diameter plus the mean diameter d_g of a glass bead ($d_{macro} \cong 6d_g$ and $d_{col} \cong 14d_{macro}$). The total pore volume V_0 is estimated to be ~103.5 mL. The

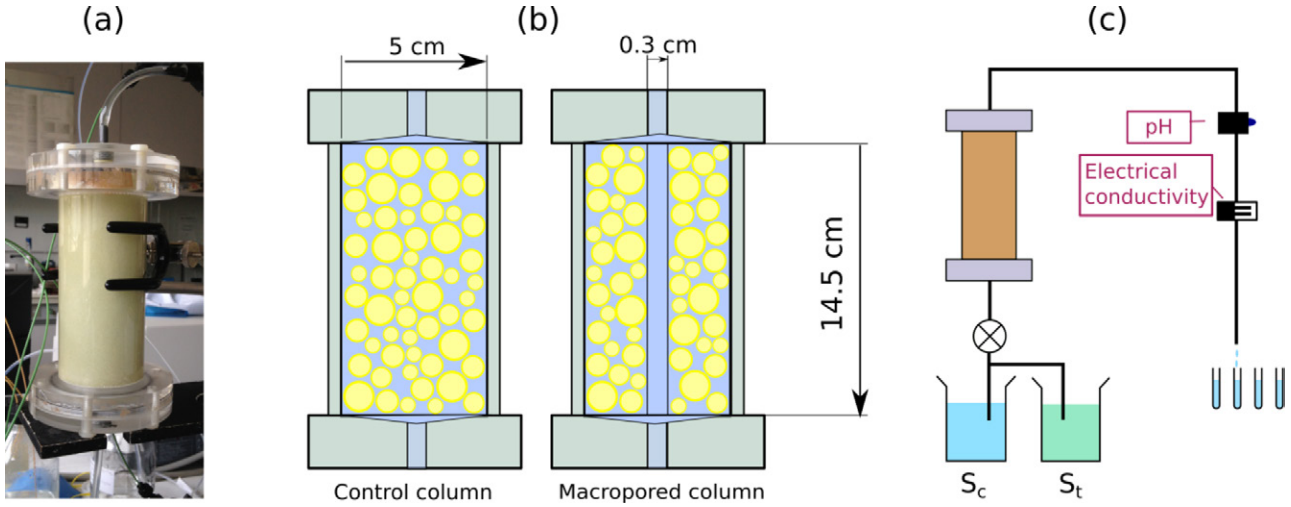

Fig. 2. (a) Experimental columns composed of glass beads, (b) schemas of the control and the macroporous columns, and (c) experimental injection setup using the Äktaprime device under saturated condition. S_c, conditioning solution; S_t, tracer solution.

assumptions outlined above are fulfilled, and, according to the theoretical analysis, $v_{mat}/v_{macro} \cong O(10^{-3})$.

Some additional experiments were performed on a vertical plastic nonporous pipe of circular cross-section, having the same dimensions as the macropore (14.5-cm length, 3-mm diameter), to study solute transfer in a macropore completely disconnected from a porous matrix.

A homogeneous control column (Column C), without any macropore, was constructed by packing in the tube of the column a mixture of glass beads and glue prior to hardening (Fig. 2b). The pore volume of Column C is 102.5 mL, and its porosity is 36%. The results obtained for this column are outlined in Appendix A.

Aqueous and Glycerol–Water Solutions

Potassium bromide was selected to perform nonreactive solute transport experiments. The Br^- ion is known to be a good tracer in soils (Haws et al., 2004) and can be quantified by ion chromatography. We confirmed that Br^- was a nonreactive species in our synthetic porous media (the sorption isotherm determined experimentally shows no adsorption on the studied porous media). Two aqueous solutions were prepared by dissolving powdered KBr in ultrapure water at concentrations of 5.0×10^{-4} mol L^{-1} (conditioning solution) and 5.0×10^{-3} mol L^{-1} (tracer solution).

Breakthrough experiments with glycerol–water solutions were performed. Glycerol ($C_3H_8O_3$) is 1.5×10^3 more viscous than pure water at 20°C. A Newtonian liquid of viscosity ranging between the viscosity of water and the viscosity of glycerol can be prepared by mixing an adequate proportion of water and glycerol (Cheng, 2008). Such a mixture can be used to decrease the molecular diffusion coefficient of Br^-. Two glycerol–water solutions (with a glycerol mass fraction of 50%) were prepared at Br^- concentrations of 5.0×10^{-4} mol L^{-1} (conditioning solution) and 5.0×10^{-3} mol L^{-1} (tracer solution). For a mass fraction of glycerol equal to 50% at 20°C, the viscosity of the glycerol–water solution is six times the viscosity of pure water (Cheng, 2008). Thus, in this glycerol–water solution, according to the Stokes–Einstein law, the coefficient of molecular diffusion D_0 of the Br^- ion is expected to be six times smaller than in pure water (in pure water at 20°C, $D_0 = 2.1 \times 10^{-9}$ m^2 s^{-1} [Bockris and Reddy, 1997]).

Injection of Solutions

Solutions were injected in the columns or in the pipe from the bottom with the help of a peristaltic pump (Ismatec ISM834A) connected to the injection system of an Äktaprime device (GE Healthcare). This liquid chromatography system was used to continuously monitor electrical conductivity, pH, UV absorbance, and temperature at the outlet of the column (Fig. 2c) or the pipe.

Elution fractions were collected to determine Br^- concentration by ion chromatography (ICS-2100, Dionex). Electrical conductivity depends linearly on Br^- concentration, with a correlation coefficient >0.95, and can thus be used to monitor Br^- elution.

The total pore volume, $V_p^{tot} = V_0 + V_{dead}$, includes the pore volume V_0 of the saturated column itself (or of the pipe) and the dead volumes of the connections (volume of water in the tubes and the column caps). The difference between V_0 and V_p^{tot} does not exceed 2% of V_0.

Prior to any experiment, the columns were saturated with the conditioning solution. A breakthrough experiment begins with the injection of three to five pore volumes of conditioning solution to stabilize the pH and the electrical conductivity. A volume of 5.0 mL of tracer solution, initially stored in the sample loop of the chromatography system, is then injected, followed by three to five pore volumes of conditioning solution to wash out the system and complete the experiment. The experiments were conducted for the following values of the volumetric flow rate (monitored at the outlet with a fraction collector): Q = 5.0, 2.0, 1.0, 0.50, 0.20, 0.10, and 0.050 mL min^{-1}. The corresponding Darcy velocities in the columns [$q = 4Q/(\pi d_{col}^2)$] were $q = 2.5 \times 10^{-1}$, 1.0×10^{-1}, 5.1×10^{-2}, 2.5×10^{-2}, 1.0×10^{-2}, 5.1×10^{-3}, and 2.5×10^{-3} cm min^{-1}. Experimental conditions are summarized in the first two rows of Table 1. Each breakthrough experiment was repeated three times (except for the smallest flow rate) to check the repeatability of the results and to quantify the experimental uncertainty.

All breakthrough experiments performed in this study were obtained under saturated conditions in a reproducible way. We did not use surface ponding to achieve saturation; we used instead a peristaltic pump to get a good liquid saturation of the columns and to set easily the value of the steady flow rate. Moreover, for Column M, the solutions were directly injected in front of the macropore to maximize the quantity of solute transported through it and the amount that can be exchanged between the macropore and the surrounding porous matrix.

Breakthrough Curves and Modeling

Breakthrough curves are easier to compare when the normalized concentration $c(t) = [C(t) - C_{min}]/(C_0 - C_{min})$, where $C(t)$ is the solute concentration at time t at the outlet, C_0 is the solute concentration in the tracer solution, and C_{min} is the solute concentration in the conditioning solution, is plotted against the number of pore volumes $V(t)/V_0$, where $V(t)$ is the volume of solution injected at time t, and V_0 is the pore volume of the system. Given the linear relationship between Br^- concentration and electrical conductivity, the normalized concentration of Br^- is equal to:

$$c(t) = \frac{\sigma(t) - \sigma_{min}}{\sigma_{max} - \sigma_{min}} \quad [3]$$

where σ_{max} is the electrical conductivity of the tracer solution, σ_{min} is the electrical conductivity at the outlet of the column during the conditioning stage, and $\sigma(t)$ is the electrical conductivity measured at time t.

All BTCs have been analyzed with the moment method (Sardin et al., 1991). The mass balance MB (i.e., the ratio of the mass of tracer having exited the column over the mass of tracer injected during the experiment) and the retardation factor $R = t_s/\tau_s$ (i.e., the ratio of the average residence time of a molecule of

Table 1. Parameters determined from the breakthrough curves of the macroporous column: mass balance (MB); retardation factor (R); convection–dispersion equation (CDE) parameters λ_{CDE} and V_{CDE}; and mobile–immobile model (MIM) parameters V_{im}, V_m, α, and λ_{MIM}. Parameter uncertainty never exceeds 5%.

Parameter	Breakthrough experiments						
Experimental conditions							
Flow rate, mL min^{-1}	0.05	0.10	0.20	0.50	1.0	2.0	5.0
Darcy velocity, cm min^{-1}	2.5×10^{-3}	5.1×10^{-3}	1.0×10^{-2}	2.5×10^{-2}	5.1×10^{-2}	1.0×10^{-1}	2.5×10^{-1}
MB	0.87	0.65	0.80	0.83	0.90	0.86	0.93
R	0.40	0.14	0.19	0.08	0.08	0.052	0.07
CDE parameters†							
λ_{CDE}, cm	20.3	22.3	8.46	4.75	3.22	3.30	1.6
V_{CDE}, mL	33.8	17.9	11.4	4.9	3.0	2.9	2.1
MIM parameters‡							
λ_{MIM}, cm	2.98	2.73	0.97	0.60	0.43	0.31	0.29
α, 10^{-3} s^{-1}	0.20	0.35	0.67	1.03	2.20	3.90	7.50
V_{im}, mL	13.6	7.8	4.3	2.6	1.9	1.7	1.6
V_m, mL	63.6	43.5	21.2	8.9	2.8	3.3	2.7

† λ_{CDE}, longitudinal dispersivity; V_{CDE}, volume of liquid involved in transport estimated by the convection–dispersion equation.
‡ λ_{MIM}, dispersivity; V_{im}, volume of the immobile region; V_m, volume of the mobile region.

solute t_s over the average residence time of a molecule of water τ_s) are related to the zeroth and first moments of experimental BTCs, $\mu_0 = \int_0^{+\infty} c(t)\mathrm{d}t$ and $\mu_1 = \int_0^{+\infty} tc(t)\mathrm{d}t$, as

$$\mathrm{MB} = \frac{\mu_0}{\delta t} \quad [4]$$

$$R = \frac{\mu_1/\mu_0 - \delta t/2}{L_{eq}\theta/q} \quad [5]$$

where δt is the duration of the injection, q is the Darcy velocity, θ is the total water content in the column, and $L_{eq} = L_{col}V_p^{tot}/V_0$ is the equivalent length of the porous system, taking into account the volume of water in caps and tubes. For a nonreactive solute, MB should be equal to 1 provided that the duration of the experiment is long enough to let all the solute get out of the system. In addition, the retardation factor is related to the volume of liquid involved in solute transport, which equals RV_0.

The nonreactive transport of Br^- is also modeled both with the convection–dispersion and with the MIMs using the HYDRUS-1D code (Hanna et al., 2012; Lamy et al., 2013; Šimůnek et al., 2005, 2008). The one-dimensional CDE solved by HYDRUS-1D is

$$\theta\frac{\partial C}{\partial t} + q\frac{\partial C}{\partial z} = \lambda q\frac{\partial^2 C}{\partial z^2} \quad [6]$$

where $C(z,t)$ is the concentration of the solute, θ is the water content, λ is the longitudinal dispersivity, and q is the Darcy velocity. The parameters fitted by HYDRUS-1D are the total water content involved in solute transport, θ_{CDE}, and the longitudinal dispersivity, λ_{CDE}. The volume of liquid involved in transport estimated by the CDE, V_{CDE}, can be deduced from the value of θ_{CDE}.

The MIM solved by HYDRUS-1D consists in the following equations:

$$\theta_m\frac{\partial C_m}{\partial t} + \theta_{im}\frac{\partial C_{im}}{\partial t} = \lambda q\frac{\partial\ C_m}{\partial} - q\frac{\partial C_m}{\partial z} \quad [7]$$

$$\theta_{im}\frac{\partial C_{im}}{\partial t} = \alpha\left(C_m - C_{im}\right) \quad [8]$$

where $C(z,t)$ is the concentration of the solute, θ is the water content (the subscript m denotes the mobile phase and im denotes the immobile phase), q is the Darcy velocity, λ is the longitudinal dispersivity, and α is the mass exchange coefficient between both phases. The parameters fitted by HYDRUS-1D are the total water content involved in solute transport $\theta_m + \theta_{im}$, the immobile water content θ_{im}, the dispersivity λ_{MIM}, and the mass exchange rate α. The pore volume $V_{MIM} = V_m + V_{im}$ (where V_{im} is the volume of the immobile region) involved in solute transport and the volume of the mobile region V_m, where advective transport takes place, can easily be deduced from θ_m and θ_{im}. Furthermore, the four MIM parameters can be used to define three characteristic times related to the processes involved in the MIM (advection, dispersion, and mass exchange): the convection time $t_{conv} = L_{eq}\theta_m/q$, the characteristic time of mass exchange between mobile and immobile water $t_\alpha = \theta_{im}/\alpha$, and the characteristic time of solute dispersion $t_d = \lambda_{MIM}\theta_m/q$ (Sardin et al., 1991). Ratios between these times make it possible to assess the relative importance between processes.

Breakthrough in the Macroporous Column and in an Isolated Macropore

Injection of Aqueous Solutions at Several Flow Rates

The normalized BTCs measured continuously for the macroporous column at different flow rates are depicted in Fig. 3. Aqueous solutions have been used to carry out these breakthrough experiments. The BTCs are strongly asymmetric, with a sharp ascent and a long descent. The breakthrough appears for small pore volumes V/V_0 (smaller than 0.02), and the normalized concentration reaches maximum values between 0.20 and 0.80. This very early breakthrough stems from the preferential flow occurring in the macropore, which constitutes a fast flow zone. Moreover, Br^- concentration nearly vanishes when the injected volume is >0.5 V_0. However, the most eye-catching result is the strong influence of the flow rate on the breakthrough. At high Darcy velocity (between 2.5×10^{-2} and 2.5×10^{-1} cm min^{-1}), the BTCs displays a single peak, whereas at lower Darcy velocity (between 2.5×10^{-3} and 1.0×10^{-2} cm min^{-1}) an inflection appears during the ascent of the BTCs. This inflection widens when the flow rate diminishes and eventually becomes a plateau for the lowest Darcy velocity (2.0×10^{-3} cm min^{-1}). This inflection suggests that the BTC becomes bimodal when the Darcy velocity is $<2.5 \times 10^{-2}$ cm min^{-1}. We explain below that this is not the case: the observed inflection is not the onset of a second peak. At low Darcy velocities ($\leq 1.0 \times 10^{-2}$ cm min^{-1}), despite the early breakthrough, the BTCs display a long tail, and more than one pore volume is required to get a stationary mass balance for the tracer, pointing at strong physical non-equilibrium effects in the macroporous column.

Mass balances, retardation factors, the CDE, and the MIM optimized parameters and related quantities for the macroporous column are listed in Table 1 and depicted in Fig. 4. The numerical BTCs corresponding to these optimized parameters are visible on the bottom part of Fig. 3. Table 1 and Fig. 4 show the influence of the flow rate on the different volumes involved in solute transport. The evolution of the pore volume involved in solute transport V_{MIM} and of the volume of the mobile region V_m with flow rate (Fig. 4) displays two distinct trends, with a threshold at 2.5×10^{-2} cm min^{-1}. However, these volumes are lower than the pore volume of the macroporous column, especially at high flow rate. Moreover, the volume of mobile water deduced from the MIM is always <15% of the pore volume of Column M, revealing that Br^- is transported through a small fraction of the water present in the column. According to the MIM, a sizeable fraction of the water in the system is not visited by the tracer and can be considered as completely isolated. This observation suggests that the presence of the macropore restricts liquid flow and solute transport in a volume encompassing the macropore but not the whole column.

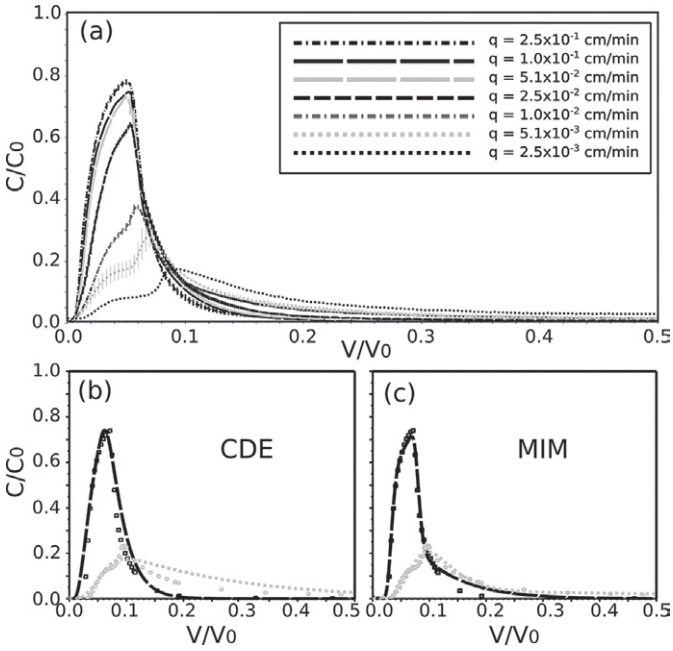

Fig. 3. (a) Influence of the flow rate of an aqueous solution on experimental Br^- breakthrough curves (BTCs) for the macroporous column (error bars represent the 95% confidence interval); (b) fitted BTCs with convection–dispersion equation (CDE) adjusted parameters for $q = 1.0 \times 10^{-1}$ cm min^{-1} and $q = 5.1 \times 10^{-3}$ cm min^{-1}; and (c) fitted BTCs with mobile–immobile model (MIM)-adjusted parameters for $q = 1.0 \times 10^{-1}$ cm min^{-1} and $q = 5.1 \times 10^{-3}$ cm min^{-1}.

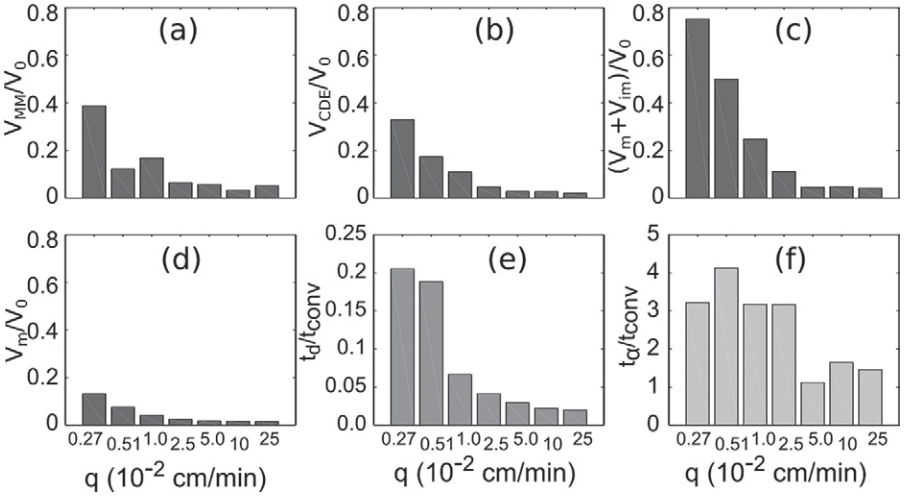

Fig. 4. Values determined from breakthrough curves by the moment method and the convection–dispersion equation (CDE) and mobile–immobile model (MIM) for the macroporous column: (a) relative volume visited by the tracer according to the moment method, (b) relative volume visited by the tracer according to the CDE model, (c) relative volume visited by the tracer according to the MIM, (d) relative volume of mobile water, (e) ratio of the characteristic time of solute dispersion to the convection time t_d/t_{conv}, and (f) ratio of characteristic time of mass exchange to the convection time t_α/t_{conv}.

Above 2.5×10^{-2} cm min^{-1}, V_m ranges between 1.5 and 2 mL; this range is very close to the volume of the macropore, which is 1.5 mL. This observation is consistent with the theoretical analysis described above: as expected on a physical basis, $V_m \cong V_{macro}$. The volume of the immobile region V_{im} lies between 2.5 and 3 mL. These values suggest that at high enough Darcy velocity, flow and solute transport are restricted to the macropore, with only a slight diffusion of solute in a small volume of water around the macropore. The ratio t_α/t_{conv} (Fig. 4) supports this interpretation: at high Darcy velocity, the immobile phase is less easily accessible to the solute, and equilibrium concentration between the mobile and immobile regions is not reached. If that were the case, the MIM would be equivalent to CDE and the goodness of fit of both models would be the same, but Fig. 3 clearly demonstrates that the MIM provides a better fit than CDE. The residence time of the mobile water in Column M is too small to achieve equilibrium within the system, confirming the results of Vanderborght et al. (2000).

Below 2.5×10^{-2} cm min^{-1}, V_{MIM} and V_m increase significantly; V_{MIM} is 10 to 75% of the pore volume of Column M (Fig. 4), and V_m ranges between 2.6 and 13.6 mL. Moreover, the ratio t_α/t_{conv} is at least twice as large as it is when $q > 2.5 \times 10^{-2}$ mL min^{-1}. These values suggest that solute transport occurs in a volume larger than the volume of the macropore and that the solute diffuses in a significant volume of immobile water (up to 60% of the pore volume of Column M).

The MIM parameters obtained with $q < 2.5 \times 10^{-2}$ cm min^{-1} are at odds with the theoretical analysis presented above. There is a tenfold increase of the volume of mobile water when q is reduced from 2.5×10^{-1} to 2.5×10^{-3} cm min^{-1}: for the highest Darcy velocity, $V_m \cong V_{macro}$, whereas for the smallest Darcy velocity $V_m \cong 10V_{macro}$. We therefore believe that the use of the MIM is questionable for the macroporous column when the flow rate becomes too small. This claim is supported by the fitted BTCs with MIM-adjusted parameters visible in Fig. 3: the goodness of MIM fit worsens when the Darcy velocity decreases. When $q = 5.1 \times 10^{-3}$ cm min^{-1}, the BTC obtained with the MIM parameters does not display the inflection observed experimentally. The tail of the experimental BTC is rather well reproduced but at the expense of the inflection part of the curve.

Injection of Glycerol–Water Solutions at Several Flow Rates

Glycerol–water solutions injected at three different flow rates (Q = 1.0, 0.50, and 0.10 mL min^{-1}, which corresponds to average Darcy velocities $q = 5.1 \times 10^{-2}$, 2.5×10^{-2}, and 5.1×10^{-3} cm min^{-1}) were used to perform additional breakthrough experiments on the macroporous column. The corresponding normalized BTCs are shown in Fig. 5. The most striking observation is how different they are from the BTCs obtained with aqueous solutions (compare Fig. 5 with Fig. 3a). First, the flow rate does not appear to have much effect on the shape of the BTCs: the three curves are similar despite the tenfold factor between the highest and the lowest flow rate. Yet, Fig. 3a shows that this spread of flow rate has a dramatic effect on the shape of the BTCs when aqueous solutions are injected. Second, the BTCs do not display inflection when the Darcy velocity is $<2.5 \times 10^{-2}$ cm min^{-1}. Third, the BTCs presented in this subsection look like the BTCs obtained with aqueous solutions at the highest Darcy velocity (2.5×10^{-1} cm min^{-1}) (Fig. 3a).

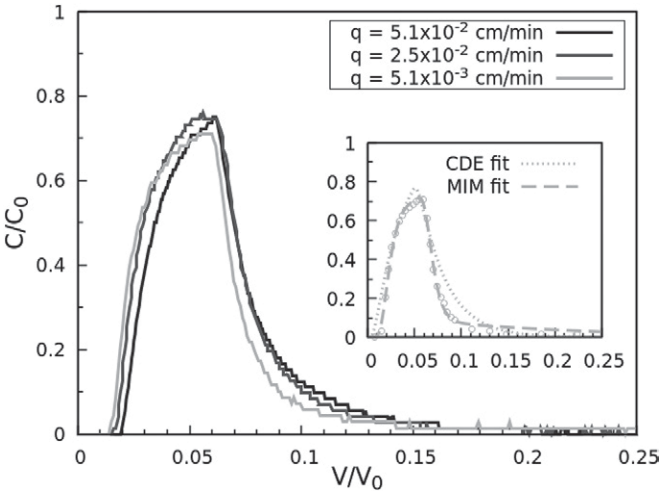

Fig. 5. Influence of the flow rate of a glycerol–water solution on experimental Br^- breakthrough curves (BTCs) for the macroporous column. Inset: Fitted BTCs with convection–dispersion equation (CDE)- and mobile–immobile model (MIM)-adjusted parameters for $q = 5.1 \times 10^{-3}$ cm min^{-1}. Symbols represent the experimental values selected for the inversion.

At the pore-scale level, the transport of Br^- is exclusively driven by advection and molecular diffusion. Thus, for a given flow rate, the diffusive component of transport is responsible for the dissimilarity of aqueous and glycerol–water BTCs. Transport of Br^- by molecular diffusion is greatly reduced in the glycerol–water solution because its viscosity is approximately six times larger than the viscosity of pure water.

As for the breakthroughs performed with aqueous solutions, CDE- and MIM-optimized parameters were derived from experimental BTCs. Numerical BTCs corresponding to these parameters are displayed in the inset of Fig. 5 for the experimental breakthrough conducted at $q = 5.1 \times 10^{-3}$ cm min^{-1}. It shows that the BTC obtained with CDE-adjusted parameters does not fit very well the experimental curve. By contrast, the BTC calculated with optimized MIM parameters is in good accordance with the experimental data (inset of Fig. 5). With the MIM, the quality of the fits does not seem to be affected by the value of the flow rate. This is a striking difference compared with what is observed when aqueous solutions are injected. In the latter case, a decrease of the flow rate is correlated with a worsening of the quality of the MIM fit. With glycerol–water solutions, the volumes of the mobile region V_m inferred for the three different flow rates range between 1.1 and 1.6 mL, very close to V_{macro}; V_m appears to be physically meaningful for a broad range of flow rates.

This set of experiments shows that the coefficient of molecular diffusion of the solute can greatly affect the shape of the BTCs.

More precisely, we believe that the diffusive mass exchange between the macropore and the porous matrix is responsible for the variation of aspect visible on the experimental BTCs when aqueous solutions are injected. When diffusive transport is strongly reduced (as is the case with glycerol–water solutions) and/or transport by advection is dominant (at high enough flow rate), solute transport is somewhat isolated in the macropore, and mass exchange with the porous matrix is limited. Glycerol–water solutions are a means to hamper this exchange, but we decided to deepen our analysis and to study what happens when mass exchange is reduced to zero along the boundary of the macropore.

Injection into a Pipe Simulating an Isolated Macropore

To investigate the effect of mass transfer between the macropore and the matrix, BTCs measured for the macroporous column were compared with those obtained with a macropore completely isolated from any surrounding porous matrix. The goal of this set of experiments is to assess the influence of the sole macropore on the breakthrough without influence of the surrounding porous matrix. Such a macropore can be simulated by a straight cylindrical tube having the same dimensions as the macropore of Column M. The experimental BTCs obtained by injection of KBr into the pipe are shown in Fig. 6a. To compare the BTCs measured on Column M and on the pipe, we normalized the volume injected into the pipe by the pore volume of Column M instead of that of the pipe itself. This choice explains the early breakthrough observed in Fig. 6a. Moreover, the comparison between the two systems has been made for similar values of the volumetric flow rate. Making the comparison for the same values of the average Darcy velocity would be irrelevant because of the strong partitioning of the flow in Column M discussed above. Indeed, according to Eq. [2], given the characteristics of Column M, 90% of water flows through the macropore.

Figure 6a shows that when the flow rate is <0.2 mL min^{-1}, the BTCs resemble the rectangular input of tracer solution injected at the inlet of the pipe (recall that 5.0 mL of tracer solution is injected at the beginning of each breakthrough experiment). When the flow rate is >1 mL min^{-1}, BTCs become asymmetric, some tailing appears, and the maximum value reached by the normalized concentration becomes lower than 1 and decreases with increasing flow rate.

The transition between these two regimes is governed by the dimensionless number $\mathcal{P} = Q/(D_0 L_{col})$; $1/\mathcal{P}$ is the ratio between the mean residence time of the solute in the macropore and the characteristic time required for the solute to diffuse transversally over a length equaling the diameter of the macropore. If $\mathcal{P} >> 1$, solute transport is dominated by advection, and breakthrough is strongly skewed, whereas if $\mathcal{P} << 1$, the breakthrough is perfectly symmetric. The latter case corresponds to the Taylor–Aris asymptotic regime, which has been thoroughly described in the literature (Aris, 1956; Taylor, 1953, 1954), and the former case corresponds to a pre-asymptotic regime (Korenaga, 1989), which is far less universal but is nevertheless well documented for straight tubes of circular cross-section. The behaviors described above are somewhat

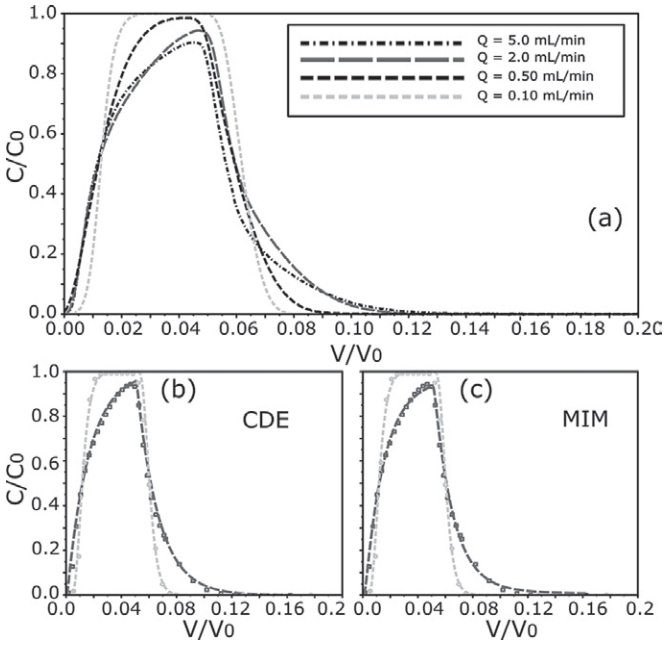

Fig. 6. (a) Influence of the flow rate of an aqueous solution on experimental Br^- breakthrough curves (BTCs) for a pipe having the same dimensions as the macropore of Column M, (b) fitted BTCs with convection–dispersion equation (CDE)-adjusted parameters for Q = 2.0 mL min^{-1} and Q = 0.10 mL min^{-1} (symbols represent the experimental values selected for the inversion), and (c) fitted BTCs with mobile–immobile model (MIM)-adjusted parameters for Q = 2.0 mL min^{-1} and Q = 0.10 mL min^{-1} (symbols represent the experimental values selected for the inversion).

smoothed by the input signal used in this study (a 5.0-mL volume of tracer solution is injected into a 1.0-mL pipe) but remain visible. Figure 6a shows that BTCs are strongly asymmetric for the two highest flow rates (the asymmetry being, as expected, even more salient for the highest flow rate) and perfectly symmetric for the two lowest flow rates. The measured BTCs look more and more similar to the input signal as the flow rate decreases because the Taylor–Aris dispersion coefficient, which is proportional to the square of the mean liquid velocity (Aris, 1956), decreases when the flow rate diminishes; the corners of the input signal are thus less eroded by dispersion at the lowest flow rate.

Figure 7 compares the BTCs obtained with Column M and the pipe. The BTCs have a similar shape for Q = 5.0 mL min^{-1}. At the highest flow rate, the macropore behaves like a pipe and can be considered as isolated from the porous matrix. The mass exchange between both zones during the breakthrough experiments is negligible or at least very limited. The small observed discrepancy may be attributed to slightly different velocity fields in the pipe and in the macropore (the macropore of Column M is not bounded by a smooth and round wall but by a packing of spherical beads), to the nonzero flow of water through the porous matrix, or to a possible small mass transfer between the macropore and the surrounding matrix.

Conversely, there is a significant difference between the BTCs of the macroporous column and the pipe at 0.10 mL min^{-1} (Fig.

7). In this case, solute transport in Column M is substantially different from what is observed in the pipe. The macropore can no longer be considered as isolated from its neighboring matrix, and the significant difference between the BTCs is likely related to the occurrence of some solute transfer between the macropore and the matrix.

The CDE- and MIM-optimized parameters have also been derived from experimental BTCs. The BTCs calculated with these parameters are shown on Fig. 6b and 6c. Physically, there is no immobile zone in a pipe undergoing a Poiseuille flow, and indeed, the measured BTCs are well reproduced by the convection–dispersion model.

The influence of molecular diffusion on solute transport can be observed with the pipe. Experimental BTCs of the pipe are affected by the viscosity of the Newtonian liquid injected to carry out the experiments (compare Fig. 8 and 6a). Modifying the nature of the liquid injected into the pipe does not modify the Poiseuille flow profile within it (at least when the Reynolds number is $<2.1 \times 10^3$ [Avila et al., 2011], which is indeed the case in our experiments), but increasing viscosity decreases the coefficient of molecular diffusion. Molecular diffusion is thus able to affect solute transport in a pipe having the same dimensions as the macropore of Column M. The decrease of molecular diffusion promotes the persistence of the pre-asymptotic regime and the skewness of the BTCs.

Discussion

Diffusive mass exchange between the macropore and the porous matrix affects solute transport in the macroporous column. However, this exchange is significant only at small Darcy velocity. Indeed, the BTCs of the macroporous column and of the pipe are similar for the highest flow rate, whatever the solutions injected. This observation is consistent with the analysis presented herein: the resemblance between the BTCs reflects the fact that, in the macroporous column, most of the liquid flows through the macropore. The BTCs of the macroporous column and of the pipe diverge when the flow rate is lowered. What really matters is the order of magnitude of the dimensionless number $\mathcal{P}$: when $\mathcal{P} >> 1$ (high flow rate and/or small coefficient of diffusion), molecular diffusion plays a negligible role on the breakthrough.

Molecular diffusion has adverse effects in the pipe and in the macroporous column. When diffusion cannot be overlooked, a non-negligible fraction of the solute will leave the macropore to enter the surrounding porous matrix. Pore velocity in the matrix being far smaller than it is in the macropore, the molecules entering the porous matrix will lag behind the ones staying in the macropore, resulting in a great variability in the residence time of solute molecules within the column. The BTCs are expected to become more skewed with increasing diffusive transport (*i.e.*, with decreasing flow rate), and this is what is observed experimentally. This should also lead to an increase of the mean residence time of the solute in the macroporous column. This prediction is consistent with the fact that the number of pore volumes corresponding to the maximum of the BTCs increases when the Darcy velocity decreases (Fig. 3a).

The effect of molecular diffusion is completely inverted for the pipe. If the mean residence time of the solute in the pipe remains moderate ($\mathcal{P} \geq 1$), each molecule of solute stays close to a given streamline and is transported at a velocity that differs from one position to another along the section of the pipe. Thus, molecules of solutes leave the pipe at broadly different times because they move at very different velocities (close to zero near the wall of the pipe and with a velocity equal to twice the average velocity on the axis of the pipe). Consequently, the corresponding BTC is very skewed and displays a long tail. A more compact and symmetric BTC is obtained when the mean residence time in the pipe is long enough ($\mathcal{P} << 1$), so that each molecule of solute can diffuse multiple times across the section of the pipe during its transport, experiencing a mix of all velocities.

Breakthrough experiments performed with aqueous solutions injected in the macroporous column have shown that the shape of the breakthrough strongly depends on the flow rate. When the Darcy velocity is lowered and becomes $<2.5 \times 10^{-2}$ cm min^{-1}, an inflection appears during the ascent of the BTC. This inflection becomes wider as the flow rate is reduced and becomes a plateau for the lowest Darcy velocity we tested. A MIM modeling is not able

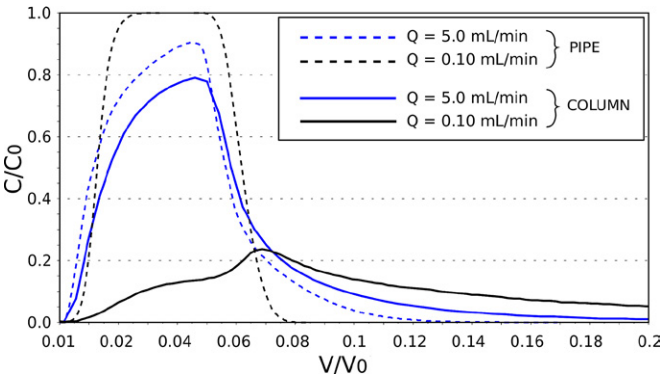

Fig. 7. Breakthrough curves of the macroporous column (continuous line) and of a pipe having the same dimensions (dotted line).

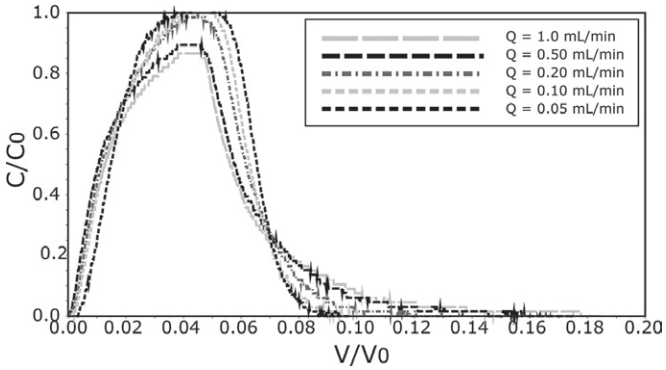

Fig. 8. Influence of the flow rate (Q) of a glycerol–water solution on experimental Br^- breakthrough curves for a pipe having the same dimensions as the macropore of Column M.

to fit accurately the experimental BTCs obtained with aqueous solutions and gives nonphysical values for the volume of mobile water when the flow rate is small enough. The observed inflection of the breakthrough cannot be reproduced with a numerical BTC derived from MIM equations: whatever the set of parameters selected, any MIM BTC will be single peaked, without any inflection. The specific feature observed in this study (ascent followed by an inflection or a plateau before a second ascent) is thus out of reach of the MIM and will remain elusive if one wants to stick to this model. We believe this is the reason why reliable information on water flow in the macroporous column cannot always be derived from the MIM; when the inflection appears, this model is not firmly grounded, and if it is used the optimized parameters obtained can have no real physical meaning. For instance, the value of the volume of mobile water results from a combination of the physical fast-moving region (i.e., the proportion of the pore space where the velocity field indicates that there is some fast flow) with an additional component linked to the volume of the pore space affected by diffusive transport.

The relative importance of molecular diffusion compared with advection in the macroporous column can be assessed thanks to the calculation of the dimensionless number $\mathcal{P}$. In this study, $\mathcal{P}$ ranges between 2.7 (for $Q = 0.05$ mL min^{-1}) and 2.7×10^2 (for $Q = 5.0$ mL min^{-1}) for the injection experiments performed with aqueous solutions. For the experiments performed with glycerol–water solutions, $\mathcal{P}$ ranges between 3.3×10^1 (for $Q = 0.10$ mL min^{-1}) and 3.3×10^2 (for $Q = 1.0$ mL min^{-1}). As discussed above, the shape of the BTCs obtained with aqueous solutions is affected by the flow rate, and a transition occurs when the value of the Darcy velocity is close to 2.5×10^{-2} cm min^{-1}. For our macroporous column, this value corresponds to a flow rate equal to 0.50 mL min^{-1} and $\mathcal{P} = 27$. The inflection visible on a few BTCs displayed in Fig. 3 clearly appears when $\mathcal{P} \leq 11$ ($q \leq 1.0 \times 10^{-2}$ cm min^{-1}). The dimensionless number $\mathcal{P}$ corresponding to the experiments performed with glycerol–water solutions was always greater than this value, and this is why the BTCs measured with glycerol–water solutions do not display an inflection.

For the macroporous column, we think that the shortcomings observed when MIM is used to fit the BTCs measured at sufficiently low $\mathcal{P}$ are related to the geometry of the pore space in macroporous media and to the way transport by molecular diffusion is modeled. Contrary to the case of soil aggregates, the fast-flow and the slow-flow regions of the macroporous column are not closely intertwined in the whole system. Solute exchange between both zones only occurs along the boundary of the macropore, and a consequent fraction of the solute present in the slow flow region (*i.e.*, in the porous matrix) can potentially be far away from the macropore and hardly accessible. Connections between the fast-flow and the slow-flow regions are rather limited and preclude MIM from producing meaningful information when some solute has entered the bulk of the porous matrix. Even the more refined model of van Genuchten et al. (1984), which has been explicitly developed to study solute transport through a soil containing a large cylindrical macropore, does not fit our experimental data very well (see Appendix B). However, when the flow rate is high enough, the transport of solute occurs in a somewhat isolated way in the macropore. In this case, a very limited fraction of solute enters the porous matrix while remaining close to the macropore, and MIM is able to accurately fit the experimental breakthroughs and to provide relevant information on water flow within the system.

Conclusions

In this study, breakthrough experiments in a macroporous column and in a pipe (having the same dimensions as the macropore present in the macroporous column) were performed by injecting KBr solutions. The pipe can be considered as a macropore isolated from any surrounding matrix. Experiments made on the macroporous column clearly show that solute transport occurs earlier in the presence of a macropore than for a homogeneous porous medium, as reported in several studies (e.g., Lamy et al., 2009).

Classical breakthrough experiments performed by injecting an aqueous solution of KBr have shown that the shape of the BTCs of the macroporous column is sensitive to the flow rate, even at a very early stage. When the flow rate is lowered, an inflection appears on the BTCs. This inflection widens and eventually becomes a plateau as Darcy velocity decreases. Additional breakthrough experiments performed by injecting a glycerol–water solution of KBr (to lower the transport rate of Br^- by molecular diffusion at a given flow rate in comparison with the case of an aqueous solution) have shown that, in this case, flow rate has little effect on the shape of the BTCs. The importance of diffusive solute transport, and thus its influence on the BTCs, depends on the value of the flow rate. The relative importance of advection and molecular diffusion for solute transport can be assessed thanks to the dimensionless number $\mathcal{P}$. When it is large enough, the shape of the BTC is not very sensitive to the precise value of $\mathcal{P}$, but this is no longer true when $\mathcal{P}$ is below a certain value: breakthrough experiments conducted by injecting aqueous solutions with $\mathcal{P} \leq 11$ yielded BTCs that strongly depended on the value of $\mathcal{P}$.

Moreover, given the characteristics of Column M, ~90% of the carrying liquid is expected to flow through the macropore, and, from a hydrodynamic point of view, the macroporous column is expected to be similar to a nonporous straight pipe of circular cross-section having the same dimensions as the macropore. When the flow rate is >1 mL min^{-1}, the BTCs measured for the macroporous column and the pipe are similar and show that the liquid flow in the pipe and the flow in the macroporous column are indeed similar and that solute transport occurs mainly within the macropore. In this case, the macropore present in the macroporous column is somewhat isolated from the surrounding porous matrix, and the solute is mainly transported through the macropore. At lower flow rate, the macropore is not acting as if it were disconnected from its neighborhood, and a fraction of the

solute is exchanged diffusively with the porous matrix, explaining the divergence observed between the BTCs of the macroporous column and the pipe (BTCs become more compact in the case of the pipe and more tailed for the macroporous column).

The MIM, a commonly used model when there is a source of nonequilibrium in a system, is not able to fit accurately the experimental BTCs of the macroporous column at low flow rate because of the presence of a plateau. In this case, MIM-optimized parameters are not physical and should not be used blindly to quantify some underlying process affecting the solute transport properties of the system. A more refined MIM-like approach (Appendix B) does not yield significantly better results. A different modeling approach, where the diffusive flux at the interface between the macropore and the porous matrix is accurately computed, is called for to simulate accurately the experimental BTCs of the macroporous column at Darcy velocities $<2.5 \times 10^{-2}$ cm min^{-1}. Even the BTCs measured at the outlet of a simple cylindrical pipe can have a quite complex shape (*e.g.*, be double-peaked), but it is necessary to resort to a detailed model to get a numerical solution in close agreement with the experimental results (Takahashi et al., 1990).

The usefulness of a detailed approach is often questioned when dealing with a soil or even a moderately complex porous media (Brusseau and Rao, 1990; Comegna et al., 2001). Whenever possible, parameters inferred from a model should be compared with orders of magnitude derived by independent means (back-of-the-envelope calculations, computer simulation, etc.) to assess the soundness of the model (Koch and Flühler, 1993; Zinn et al., 2004). If its validity is doubtful, the principle of parameter parsimony should prevail and foster the use of a simpler model, such as the CDE (Comegna et al., 2001).

Verifying the plausibility of some parameters is simpler when working with a model porous media under saturated conditions than it is for an unsaturated soil. If one wants to see more often independent checking of the parameters inferred from a BTC, a good understanding on how water flows in a column containing a given realistic soil is required. Different imaging techniques (CT scan, MRI) are available and can contribute to reaching that goal (Werth et al., 2010). Combined with computer simulations, these techniques can help to improve our knowledge of the dynamics of water in complex porous media under conditions representative of the functioning of a soil.

Appendix A

Breakthrough in the Matrix (Control Column)

The BTCs obtained for the control column by injection of an aqueous solution at different flow rates are displayed in Fig. A1. Unlike what has been observed with the macroporous column, the BTCs obtained for the control column are roughly symmetric. Breakthroughs start around $V/V_0 = 0.8$ and reach their maximum values between 1.1 and 1.2 V_0. Maximum values of C/C_0 are between 0.13 and 0.18, much lower than in the case of the macroporous column. The value of the flow rate has a slight influence on

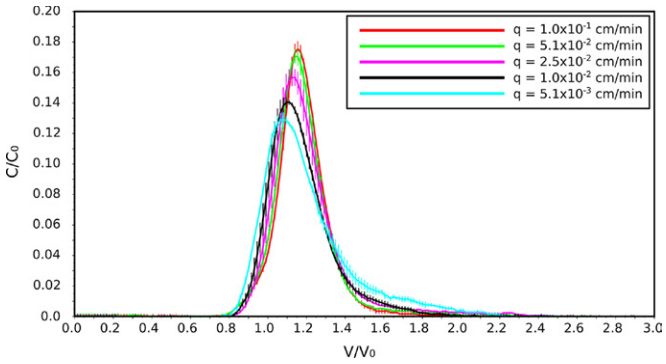

Fig. A1. Normalized breakthrough curves of KBr in the control column for different flow rates.

the BTCs, albeit far less obvious than for the macroporous column: when the flow rate decreases, the BTCs become more asymmetric (i.e., they display a longer tail), hinting at the existence of a growing fraction of immobile water within the control column. Moreover, at low flow rate, the BTC increases more rapidly and reaches a maximum value smaller than at higher flow rate.

As for the macroporous column, mass balances, retardation factors, and optimized parameters have been calculated for CDE and MIM. The mass balances ($\cong$1) indicate that the solute completely exits the control column. The retardation factor does not evolve with the flow rate and is slightly larger than 1 (between 1.14 and 1.18), leading to a volume involved in solute transport RV_0 slightly larger than the pore volume of the control column. Batch experiments have shown that Br^- did not sorb onto the solid phase (*i.e.*, the mixture of glass beads and glue). We believe that this discrepancy may be due to the presence of a small volume without any beads near the exit of Column C. It could also explain why the BTCs reach their maximum values after slightly more than one pore volume.

The CDE and MIM parameters were also calculated. As with the method of moments, the volume of water involved in solute transport remains the same whatever the flow rate and is approximately equal to the pore volume of the column. The dispersivity and the mass exchange rate also remain roughly constant. Consequently, the ratio t_α/t_{conv} increases with increasing Darcy velocity, whereas t_d/t_{conv} does not change.

Overall, the BTCs of Column C are consistent with what is expected when a nonreactive solute is transported through a homogenous porous medium. The shape of the normalized effluent curves is well reproduced by the CDE and remains invariant for a wide range of flow rates.

Appendix B

Comparison between the Breakthrough Curves in the Macroporous Column and the Model of van Genuchten et al. (1984)

Van Genuchten et al. (1984) devised a MIM-like model of solute transport through a cylindrical macropore of radius

$r_{macro} = d_{macro}/2$, embedded in a soil matrix filling a hollow cylinder of inner radius r_{macro} and outer radius $r_{col} = d_{col}/2$, with simultaneous radial diffusion from the boundary of the large pore into the surrounding porous soil matrix (van Genuchten et al., 1984). Using the notations used in Eq. [7] and the coefficient of longitudinal dispersion D_m instead of the longitudinal dispersivity λ, the first equation of their model is:

$$\theta_m \frac{\partial C_m}{\partial t} + \theta_{im} \frac{\partial C_{im}}{\partial t} = \theta_m D_m \frac{\partial^2 C_m}{\partial z^2} - q \frac{\partial C_m}{\partial z}$$

However, unlike in the classical MIM, the concentration of the solute in the immobile phase C_{im} is not a fundamental quantity of their model because it is defined as an average concentration:

$$C_{im}(z,t) = \frac{2}{r_{col}^2 - r_{macro}^2} \int_{r_{macro}}^{r_{col}} r C_a(z,r,t)\,dr$$

where C_a is the local concentration of solute in the porous matrix. Solute transport in this part of the system is modeled with the cylindrical diffusion equation, with a Dirichlet boundary condition along the inner boundary and a Neumann boundary condition along the outer boundary of the hollow cylinder:

$$\frac{\partial C_a}{\partial t} = \frac{D_0}{r} \frac{\partial}{\partial r}\left(r \frac{\partial C_a}{\partial r} \right) \qquad r_{macro} \le r \le r_{col},$$

$$C_a(z, r_{macro}, t) = C_m(z,t), \quad \frac{\partial C_a}{\partial r}(z, r_{col}, t) = 0$$

This model can be solved analytically. The exact solution is rather involved, but van Genuchten et al. (1984) found an expression that they claim to be a good approximation of the exact solution (see Eq. 95 in van Genuchten et al. [1984]). With this expression, we calculated the BTCs predicted by the model for the macroporous column. With our notations, assuming that the liquid flows entirely through the macropore, this approximate solution yields the following expression for the normalized concentration at the outlet of the macroporous column when a volume of tracer solution (V_{inj}) is injected at the onset of the breakthrough experiments:

$$c(v) = c_{step}(v) - c_{step}\left(v - \frac{V_{inj}}{V_0} \right) \qquad [B1]$$

where v is the number of pore volumes $V(t)/V_0$, and c_{step} is determined as

$$c_{step}(v) = H\left(v - \frac{\pi d_{macro}^2 L_{col}}{4Q} \right) \exp\left(-\frac{\pi \phi D_0 L_{col}}{Q} \right) \times \operatorname{erfc}\left[\frac{1}{2} \pi \phi L_{col} d_{macro} \left(\frac{D_0}{QV_0} \frac{1}{v - \pi d_{macro}^2 L_{col}/4Q} \right)^{1/2} \right] \qquad [B2]$$

where H is the Heavyside step function.

Two simulated BTCs are displayed in Fig. B1 and can be compared with the experimental BTCs depicted in Fig. 3a. The apparition of the plateau and the shift of the peak is not reproduced for the lowest value of the Darcy velocity by the model of van Genuchten et al. (1984). The numerical BTC calculated for the highest value of the Darcy velocity shares some similarities with the corresponding experimental BTC, but, even in this case, the agreement between the model and the experiment is not perfect.

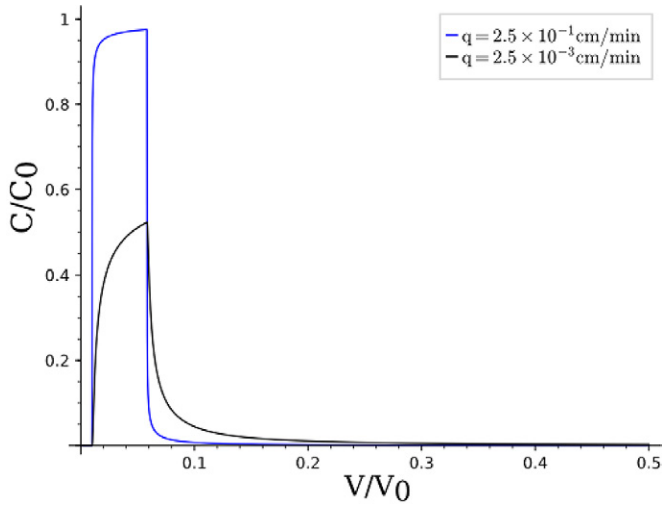

Fig. B1. Breakthrough curves calculated from Eq. [B1] and [B2] with injected volume V_{inj} = 5 mL for two different Darcy velocities, $q = 2.1 \times 10^{-1}$ cm min^{-1} and $q = 2.1 \times 10^{-3}$ cm min^{-1}.

Acknowledgments

We thank the technical staff of laboratoire Navier for help constructing the columns and D. Demare, N. Caubrière, and C. Ragoin from the analytical division of laboratoire Eau et Environnement (IFSTTAR) for their support.

References

Allaire, S.E., S.C. Gupta, J. Nieber, and J.F. Moncrief. 2002. Role of macropore continuity and tortuosity on solute transport in soils: 2. Interactions with model assumptions for macropore description. J. Contam. Hydrol. 58:283–298. doi:10.1016/S0169-7722(02)00034-7

Allaire, S.E., S. Roulier, and A.J. Cessna. 2009. Quantifying preferential flow in soils: A review of different techniques. J. Hydrol. 378:179–204. doi:10.1016/j.jhydrol.2009.08.013

Aris, R. 1956. On the dispersion of a solute in a fluid flowing through a tube. Proc. R. Soc. London, Ser. A 235:67–77. doi:10.1016/S1874-5970(99)80009-5

Arthur, J.K., D.W. Ruth, and M.F. Tachie. 2009. PIV measurements of flow through a model porous medium with varying boundary conditions. J. Fluid Mech. 629:343–374. doi:10.1017/S0022112009006405

Avila, K., D. Moxey, A. de Lozar, M. Avila, D. Barkley, and B. Hof. 2011. The onset of turbulence in pipe flow. Science 333:192–196. doi:10.1126/science.1203223

Bear, J. 1972. Dynamics of fluids in porous media. Dover Publ., Mineola, NY.

Beavers, G.S., and D.D. Joseph. 1967. Boundary conditions at a naturally permeable wall. J. Fluid Mech. 30:197–207. doi:10.1017/S0022112067001375

Berkowitz, B. 1989. Boundary conditions along permeable fracture walls: Influence on flow and conductivity. Water Resour. Res. 25:1919–1922. doi:10.1029/WR025i008p01919

Berkowitz, B. and H. Scher. 2009. Exploring the nature of non-Fickian transport in laboratory experiments. Adv. Water Resour. 32:750–755. doi:10.1016/j.advwatres.2008.05.004

Berkowitz, B., A. Cortis, M. Dentz, and H. Scher. 2006. Modeling non-Fickian transport in geological formations as a continuous time random walk. Rev. Geophys. 44:RG2003. doi:10.1029/2005rg000178

Berkowitz, B., S. Emmanuel, and H. Scher. 2008. Non-Fickian transport and multiple-rate mass transfer in porous media. Water Resour. Res. 44:W03402. doi:10.1029/2007wr005906

Beven, K., and P. Germann. 1982. Macropores and water flow in soils. Water Resour. Res. 18:1311–1325. doi:10.1029/WR018i005p01311

Beven, K., and P. Germann. 2013. Macropores and water flow in soils revisited. Water Resour. Res. 49:3071–3092. doi:10.1002/wrcr.20156

Bijeljic, B. and M.J. Blunt. 2006. Pore-scale modeling and continuous time random walk analysis of dispersion in porous media. Water Resour. Res. 42:W01202. doi:10.1029/2005wr004578

Bockris, J., and A. Reddy. 1997. Modern electrochemistry 1: Ionics. Springer, Berlin.

Brusseau, M., and P. Rao. 1990. Modeling solute transport in structured soils: A review. Geoderma 46:169–192. doi:10.1016/0016-7061(90)90014-Z

Brusseau, M.L. 1993. The influence of solute size, pore water velocity, and intraparticle porosity on solute dispersion and transport in soil. Water Resour. Res. 29:1071–1080. doi:10.1029/92WR02595

Cheng, N.-S. 2008. Formula for the viscosity of a glycerol–water mixture. Ind. Eng. Chem. Res. 47:3285–3288. doi:10.1021/ie071349z

Cihan, A., and J.S. Tyner. 2011. 2-D radial analytical solutions for solute transport in a dual-porosity medium. Water Resour. Res. 47:W04507. doi:10.1029/2009WR008969

Coats, K., and B. Smith. 1964. Dead-end pore volume and dispersion in porous media. Soc. Pet. Eng. J. 4:73–84. doi:10.2118/647-PA

Comegna, V., A. Coppola, and A. Sommella. 2001. Effectiveness of equilibrium and physical non-equilibrium approaches for interpreting solute transport through undisturbed soil columns. J. Contam. Hydrol. 50:121–138. doi:10.1016/S0169-7722(01)00100-0

Czapar, G., R. Horton, and R. Fawcett. 1992. Herbicide and tracer movement in soil columns containing an artificial macropore. J. Environ. Qual. 21:110–115. doi:10.2134/jeq1992.00472425002100010016x

Desmond, K.W., and E.R. Weeks. 2014. Influence of particle size distribution on random close packing of spheres. Phys. Rev. E 90:022204. doi:10.1103/PhysRevE.90.022204

Di Pietro, L., S. Ruy, and Y. Capowiez. 2003. Predicting preferential water flow in soils by traveling-dispersive waves. J. Hydrol. 278:64–75. doi:10.1016/S0022-1694(03)00124-0

Farr, R.S., and R.D. Groot. 2009. Close packing density of polydisperse hard spheres. J. Chem. Phys. 131:244–104. doi:10.1063/1.3276799

Gerke, H.H. 2006. Preferential flow descriptions for structured soils. J. Plant Nutr. Soil Sci. 169:382–400. doi:10.1002/jpln.200521955

Gerke, H.H., and J.M. Köhne. 2004. Dual-permeability modeling of preferential bromide leaching from a tile-drained glacial till agricultural field. J. Hydrol. 289:239–257. doi:10.1016/j.jhydrol.2003.11.019

Ghodrati, M., M. Chendorain, and Y.J. Chang. 1999. Characterization of macropore flow mechanisms in soil by means of a split macropore column. Soil Sci. Soc. Am. J. 63:1093–1101. doi:10.2136/sssaj1999.6351093x

Griffioen, J.W., D.A. Barry, and J.-Y. Parlange. 1998. Interpretation of two-region model parameters. Water Resour. Res. 34:373–384. doi:10.1029/97WR02027

Hanna, K., L. Lassabatere, and B. Bechet. 2012. Transport of two naphthoic acids and salicylic acid in soil: Experimental study and empirical modeling. Water Res. 46:4457–4467. doi:10.1016/j.watres.2012.04.037

Haws, N.W., B.S. Das, and P.S.C. Rao. 2004. Dual-domain solute transfer and transport processes: Evaluation in batch and transport experiments. J. Contam. Hydrol. 75:257–280. doi:10.1016/j.jconhyd.2004.07.001

Hu, Q., and M.L. Brusseau. 1995. Effect of solute size on transport in structured porous media. Water Resour. Res. 31:1637–1646. doi:10.1029/95WR01138

Khan, A.U.-H., and W.A. Jury. 1990. A laboratory study of the dispersion scale effect in column outflow experiments. J. Contam. Hydrol. 5:119–131. doi:10.1016/0169-7722(90)90001-W

Koch, S., and H. Flühler. 1993. Solute transport in aggregated porous media: Comparing model independent and dependent parameter estimation. Water Air Soil Pollut. 68:275–289. doi:10.1007/BF00479408

Köhne, J.M., S. Köhne, and J. Šimůnek. 2009. A review of model applications for structured soils: A. Water flow and tracer transport. J. Contam. Hydrol. 104:4–35. doi:10.1016/j.jconhyd.2008.10.002

Korenaga, T. 1989. An experimental study of the dispersion in laminar tube flow. AIChE J. 35:1395–1398. doi:10.1002/aic.690350821

Lafolie, F., C. Hayot, and D. Schweich. 1997. Experiments on solute transport in aggregated porous media: Are diffusions within aggregates and hydrodynamic dispersion independent? Transp. Porous Media 29:281–307. doi:10.1023/A:1006513725029

Lamy, E., L. Lassabatere, B. Bechet, and H. Andrieu. 2009. Modeling the influence of an artificial macropore in sandy columns on flow and solute transfer. J. Hydrol. 376:392–402. doi:10.1016/j.jhydrol.2009.07.048

Lamy, E., L. Lassabatere, B. Bechet, and H. Andrieu. 2013. Effect of a nonwoven geotextile on solute and colloid transport in porous media under both saturated and unsaturated conditions. Geotext. Geomembr. 36:55–65. doi:10.1016/j.geotexmem.2012.10.009

Larsson, M., N. Jarvis, G. Torstensson, and R. Kasteel. 1999. Quantifying the impact of preferential flow on solute transport to tile drains in a sandy field soil. J. Hydrol. 215:116–134. doi:10.1016/S0022-1694(98)00265-0

Lassabatere, L., T. Winiarski, and R. Galvez-Cloutier. 2004. Retention of three heavy metals (Zn, Pb, and Cd) in a calcareous soil controlled by the modification of flow with geotextiles. Environ. Sci. Technol. 38:4215–4221. doi:10.1021/es035029s

Li, J.C.M., and P. Chang. 1955. Self-diffusion coefficient and viscosity in liquids. J. Chem. Phys. 23:518–520. doi:10.1063/1.1742022

Li, Y., and M. Ghodrati. 1997. Preferential transport of solute through soil columns containing constructed macropores. Soil Sci. Soc. Am. J. 61:1308–1317. doi:10.2136/sssaj1997.03615995006100050004x

Neretnieks, I. 1980. Diffusion in the rock matrix: An important factor in radionuclide retardation? J. Geophys. Res. 85(B8):4379–4397. doi:10.1029/jb085ib08p04379

Perret, J., S.O. Prasher, A. Kantzas, and C. Langford. 2000. A two-domain approach using CAT scanning to model solute transport in soil. J. Environ. Qual. 29:995–1010. doi:10.2134/jeq2000.00472425002900030039x

Phillips, R.E., J.M. Zeleznik, G.H. Dunn, and V.L. Quisenberry. 1989. Mechanism of water entry into simulated macropores. Soil Sci. Soc. Am. J. 53:1629–1635. doi:10.2136/sssaj1989.03615995005300060003x

Rao, P.S.C., R.E. Jessup, D.E. Rolston, J.M. Davidson, and D.P. Kilcrease. 1980a. Experimental and mathematical description of nonadsorbed solute transfer by diffusion in spherical aggregates. Soil Sci. Soc. Am. J. 44:684–688. doi:10.2136/sssaj1980.03615995004400040004x

Rao, P.S.C., D.E. Rolston, R.E. Jessup, and J.M. Davidson. 1980b. Solute transport in aggregated porous media: Theoretical and experimental evaluation. Soil Sci. Soc. Am. J. 44:1139–1146. doi:10.2136/sssaj1980.03615995004400060003x

Rao, P.S.C., R.E. Jessup, and T.M. Addiscott. 1982. Experimental and theoretical aspects of solute diffusion in spherical and nonspherical aggregates. Soil Sci. 133:342–349. doi:10.1097/00010694-198206000-00002

Rosenbom, A.E., R. Therrien, J.C. Refsgaard, K.H. Jensen, V. Ernstsen, and K.E.S. Klint. 2009. Numerical analysis of water and solute transport in variably-saturated fractured clayey till. J. Contam. Hydrol. 104:137–152. doi:10.1016/j.jconhyd.2008.09.001

Saravanathiiban, D., M. Kutay, and M. Khire. 2014. Effect of macropore tortuosity and morphology on preferential flow through saturated soil: A lattice Boltzmann study. Comput. Geotech. 59:44–53. doi:10.1016/j.compgeo.2014.02.006

Sardin, M., D. Schweich, F.J. Leu, and M.Th. van Genuchten. 1991. Modeling the nonequilibrium transport of linearly interacting solutes in porous media: A review. Water Resour. Res. 27:2287–2307. doi:10.1029/91WR01034

Seyfried, M.S., and P.S.C. Rao. 1987. Solute transport in undisturbed columns of an aggregated tropical soil: Preferential flow effects. Soil Sci. Soc. Am. J. 51:1434–1444. doi:10.2136/sssaj1987.03615995005100060008x

Šimůnek, J., M.Th. van Genuchten, and M. Šejna. 2005. The HYDRUS-1D software package for simulating the one-dimensional movement of water, heat, and multiple solutes in variably-saturated media. Res. Rep. 3. Univ. of California, Riverside.

Šimůnek, J., M.Th. van Genuchten, and M. Šejna. 2008. Development and applications of the HYDRUS and STANMOD software packages and related codes. Vadose Zone J. 7:587–600. doi:10.2136/vzj2007.0077

Sudicky, E.A., R.W. Gillham, and E.O. Frind. 1985. Experimental investigation of solute transport in stratified porous media: 1. The nonreactive case. Water Resour. Res. 21:1035–1041. doi:10.1029/wr021i007p01035

Takahashi, T., T. Korenaga,, and F. Shen. 1990. A numerical solution for the dispersion in laminar flow through a circular tube. Can. J. Chem. Eng. 68:191–196. doi:10.1002/cjce.5450680202

Tang, D.H., E.O. Frind, and E.A. Sudicky. 1981. Contaminant transport in fractured porous media: Analytical solution for a single fracture. Water Resour. Res. 17:555–564. doi:10.1029/wr017i003p00555

Taylor, G. 1953. Dispersion of soluble matter in solvent flowing slowly through a tube. Proc. R. Soc., Ser. A 219:186–203. doi:10.1098/rspa.1953.0139

Taylor, G. 1954. Conditions under which dispersion of a solute in a stream of solvent can be used to measure molecular diffusion. Proc. R. Soc., Ser. A 225:473–477. doi:10.1098/rspa.1954.0216

Vanderborght, J., A. Timmerman, and J. Feyen. 2000. Solute transport for steady-state and transient flow in soils with and without macropores. Soil Sci. Soc. Am. J. 64:1305–1317. doi:10.2136/sssaj2000.6441305x

Vanderborght, J., P. Gähwiller, and H. Flühler. 2002. Identification of transport processes in soil cores using fluorescent tracers. Soil Sci. Soc. Am. J. 66:774–787. doi:10.2136/sssaj2002.7740

van Genuchten, M.Th., D.H. Tang, and R. Guennelon. 1984. Some exact solutions for solute transport through soils containing large cylindrical macropores. Water Resour. Res. 20:335–346. doi:10.1029/WR020i003p00335

van Genuchten, M.Th., and P. Wierenga. 1976. Mass transfer studies in sorbing porous media: I. Analytical solutions. Soil Sci. Soc. Am. J. 40:473–480. doi:10.2136/sssaj1976.03615995004000040011x

Vogel, H.-J., I. Cousin, O. Ippisch, and P. Bastian. 2006. The dominant role of structure for solute transport in soil: Experimental evidence and modelling of structure and transport in a field experiment. Hydrol. Earth Syst. Sci. 10:495–506. doi:10.5194/hess-10-495-2006

Wan, J., T.K. Tokunaga, C.-F. Tsang, and G.S. Bodvarsson. 1996. Improved glass micromodel methods for studies of flow and transport in fractured porous media. Water Resour. Res. 32:1955–1964. doi:10.1029/96WR00755

Weiler, M. 2005. An infiltration model based on flow variability in macropores: Development, sensitivity analysis and applications. J. Hydrol. 310:294–315. doi:10.1016/j.jhydrol.2005.01.010

Werth, C.J., C. Zhang, M.L. Brusseau, M. Oostrom, and T. Baumann. 2010. A review of non-invasive imaging methods and applications in contaminant hydrogeology research. J. Contam. Hydrol. 113:1–24. doi:10.1016/j.jconhyd.2010.01.001

Zehe, E., and H. Flühler. 2001. Preferential transport of isoproturon at a plot scale and a field scale tile-drained site. J. Hydrol. 247:100–115. doi:10.1016/S0022-1694(01)00370-5

Zinn, B., L.C. Meigs, C.F. Harvey, R. Haggerty, W.J. Peplinski, and C.F. von Schwerin. 2004. Experimental visualization of solute transport and mass transfer processes in two-dimensional conductivity fields with connected regions of high conductivity. Environ. Sci. Technol. 38:3916–3926. doi:10.1021/es034958g